THE JOURNAL OF PHYSICAL CHEMISTRY C

Article

pubs.acs.org/JPCC

Structural Features and Electronic Properties of MgO Nanosheets and Nanobelts

Y. G. Zhang,[†] H. Y. He,*[,†] and B. C. Pan[†,‡]

[†]Department of Physics and [‡]Hefei National Laboratory for Physical Sciences at Microscale, University of Science and Technology of China, Hefei, Anhui 230026, PR China

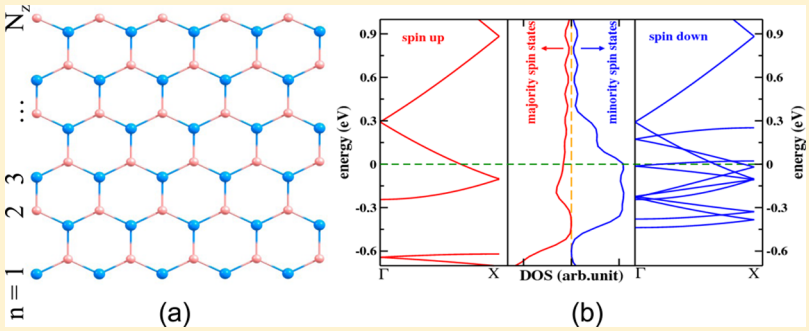

ABSTRACT: On the basis of first principles calculations, we systematically investigate the structural features, stabilities, and electronic properties of the MgO nanosheets and corresponding nanobelts with different widths. For the MgO(100) sheet, two new kinds of structures characterizing rumpling and wavelike features are found to be more stable than the flat one. Our calculations predict that these two kinds of MgO(100) and MgO(111) nanosheets exhibit semiconductive properties, with the band gaps varying from 4.23 to 4.38 eV. Moreover, their band gaps vary as different functions of the applied strain. In addition, we find that the MgO(111) nanobelts with zigzag edges show metallic behavior whereas the MgO(111) nanobelts with armchair edges and MgO(100) nanobelts exhibit semiconductive properties. In particular, the band gaps for the semiconductive nanobelts can be manipulated from 2.75 to 3.95 eV by the width of the nanobelts. These aspects provide these nanobelts with promising applications in spintronics and nanoscaled ultraviolet photoelectronic devices.

I. INTRODUCTION

Low-dimensional nanostructures have attracted a wide range of research interest in the field of materials science because of their exceptional nanoscale structures and extraordinary properties.[1−4] Recently, different nanostructures such as nanosheets, nanowires, and nanobelts of various materials have been intensively explored in both experimental and theoretical areas.[5−9] Among these nanostructural materials, the MgO nanocrystalline structure has attracted increasing attention because of its significant performance as unreactive substrates and model catalysts.[10−12] More importantly, MgO possesses a wide band gap of about 7.8 eV and smooth surface features, which allow it to act as persistent photoelectronic applications in photoelectrochemical solar cells, metal oxide semiconductor gate-controlled devices, and high-temperature superconductor composites.[10,13,14]

Until now, much effort has been devoted to synthesizing MgO ultrathin films and nanosheets, motivated by the achievement of graphene and its novel properties.[15−18] Both of the polar (111) and nonpolar (100) facets of MgO thin films with high crystalline quality have been successfully synthesized on different substrates from layer-by-layer epitaxial growth in the experiments.[19,20] It was found that MgO(111) films possess atomically flat surfaces.[19] However, the surfaces of the ultrathin films, or monolayers, exhibit new features. For example, it was theoretically predicted that MgO monolayers deposited on Ag substrates were rumpling, and it was revealed that such rumpling of supported oxide films was a structural response to the interfacial charge transfer.[21] Besides, MgO(001) and MgO(111) monolayer islands were achieved from different deposition temperatures and oxygen partial pressures in experiments.[22]

Previous reports on MgO nanosheets (a few layers or a monolayer) mainly focused on the behaviors of the sheet on different substrates. In fact, the properties of free-standing monolayers are important in understanding their properties. However, the MgO(111) monolayer features graphene-like (hexagonal) structures, so MgO(111) nanobelts also possess two kinds of edges: zigzags and armchairs. The electronic structures of these nanobelts with different widths are still puzzling.

The aim of this work is to explore the stabilities and the electronic structures of both MgO(111) and MgO(100) monolayers and the corresponding nanobelts. Our calculations demonstrate that the polar MgO(111) nanosheet retains its graphene-like structure, and the flat nonpolar MgO(100)

Received: August 3, 2012
Revised: September 21, 2012
Published: October 3, 2012

nanosheet is either rumpled or wavelike. All of these stable nanosheets exhibit semiconductive properties, with similar band gaps of about 4.3 eV. Moreover, the electronic structures of the corresponding nanobelts are revealed to be dependent on the facets, edge features, and width of the nanobelts. Such modulation of the band gaps provides MgO nanobelts with promising applications in nanodevices.

II. COMPUTATIONAL DETAILS

Density functional theory with a local density approximation implanted in the SIESTA package[23−25] is employed for the structural optimization and total energy calculations. The norm-conserving pseudopotentials generated by using the Troullier−Martins scheme[26] are employed to describe the interaction of valence electrons, which is expressed in a fully separable form developed by Kleiman and Bylander.[27,28] The exchange-correlation potential in Perdew−Zunger form is adopted. The split-valence double-ζ plus polarization orbitals are chosen for Mg and O atoms, and Brillouin zone sampling is carried out with a 4 × 4 × 1 Monkhorst−Pack grid. The conjugate gradient algorithm is adopted to relax the structures fully until the residual force acting on each atom is no more than 0.01 eV/Å.

The supercells of the MgO(111) sheet and the MgO(100) sheet consist of 8 × 8 and 5 × 5 primary unit cells, respectively. A vacuum region greater than 15 Å perpendicular to the sheet (along the z axis) is applied to avoid the interaction between images caused by the periodic boundary condition. For the nanobelts, the chosen supercell in each case consists of three or four primary unit cells in the periodic directions. In our calculations, the lattice constants and the atomic positions of the concerned systems are fully optimized.

III. RESULTS AND DISCUSSION

A. Stabilities and Electronic Structures of MgO(111) and MgO(100) Nanosheets. To begin, we construct the atomic structure of MgO nanosheets (NSs) oriented along either the (111) or (100) direction. For the polar MgO(111) monolayer, we adopt the planar graphene-like structure that has been reported to be the most stable structure for the (111) facet.[5] For the nonpolar MgO (100) monolayer, it is generated from the rock-salt-structured MgO bulk. After full relaxation, the obtained configurations retain the hexagonal (for MgO(111)) and the square (for MgO(100)) symmetries, as shown in Figure 1a,b. The lattice constants for the MgO(111) sheet and the MgO(100) sheet are 3.18 and 3.85 Å, respectively, and are comparable to the previously reported values (3.26 and 4.01 Å).[5,29]

To examine the mechanical stabilities of these structures further, the phonon spectra analysis has also been carried out for each case. Our results show that there is no imaginary frequency in phonon spectra for the MgO(111) monolayer, indicating the mechanical stability of the MgO(111) NS with hexagonal structure. In contrast, there are a few imaginary frequencies in the phonon spectra for the planar MgO(100) NS, implying the mechanical instability of this case. To remove these imaginary frequencies and then attain a virtually stable configuration, the system is further optimized so that the eigenvectors of the imaginary frequency are taken into account. Finally, no imaginary frequency is found in the phonon spectra of the optimized configuration, and a virtually stable system is obtained. By examining the obtained structures, we surprisingly find that the initial MgO(100) NS with Mg atoms and O atoms in the same plane converts to a rumpled configuration eventually. This rumpling monolayer exhibits a microscopic washboard structural feature, where O atoms remain in the initial plane and Mg atoms deviate from the plane by about 0.3 or −0.3 Å oppositely and alternately in lines, as shown in Figure 1c. It should be noted that such up- and down-rumpling behaviors are displayed along both in-plane x and y axes. For convenience, we denote such a structural nanosheet as the MgO(100)-rumpling sheet.

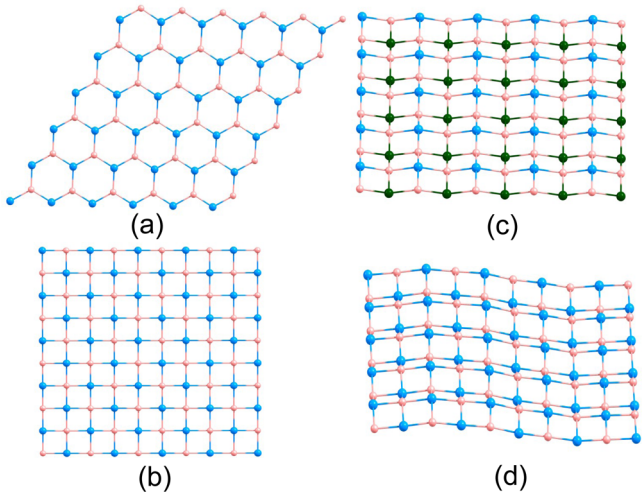

Figure 1. (Color online) The atomic structure of MgO (111) (a), MgO(100)-flat (b), MgO(100)-rumpling (c) and MgO(100)-wave (d) nanosheets. The blue (green) balls and the red balls represent the Mg and the O atoms, respectively. The green balls and the blue balls in (b) stand for the Mg atoms in different planes.

It is necessary to note that these rumpling structural features are different from that of the MgO(100) monolayer epitaxially grown on the Ag substrate in which the buckling feature appeared only along one periodic direction.[21] The equilibrium lattice constant of this rumpling configuration is about 3.79 Å, a little contraction with respect to that of the flat one. Compared to that of the flat one, the cohesive energy of the system decreases by about 0.22 eV per Mg−O pair, which indicates that this rumpling configuration is more stable than the flat one.

More interestingly, during optimization, we obtain another geometry of the MgO(100) sheet by applying a biaxial isotropic strain. Different from the rumpling MgO(100) sheet with buckling Mg−O bonds along two periodic directions, this MgO(100) sheet retains the same rumpling feature in one periodic direction while showing wavelike character in another periodic direction. This kind of nanosheet is denoted as a MgO(100)-wave sheet, and its configuration is shown in Figure 1d. The calculated phonon spectra show that there is no imaginary frequency, indicating that this configuration is also stable. The lattice constant of this MgO(100)-wave sheet is about 3.76 Å, which is very close to that of the rumpling one. The formation energy of this new nanosheet is almost degenerate with the rumpling one, with an energy difference of less than 1.0 meV/ atom. In addition, we find that when the lattice constant exceeds to the value of 3.84 Å, the wavelike structure completely converts to the rumpling one.

It is noted that such a wave structural character is similar to that of the free-standing bilayer graphane observed in the experiment,[30] where the wavelengths were variable between 3.6 and 6.4 Å. Inspired by such structural features of the bilayer

dx.doi.org/10.1021/jp3077062 | J. Phys. Chem. C 2012, 116, 23130−23135

graphane, we wonder whether there is a specific wavelength in this wavelike NS and how the stability of the system is dependent on the wavelength. For this purpose, we adopt MgO(100)-wave sheets with seven different wavelengths (3, 4, 6, 7, 9, 11, and 14 times the lattice constant) to explore their stabilities. Our calculations show that the formation energies of these NSs with different wavelengths are very close to each other, with energy difference of less than 21 meV/ Mg−O pair. This implies that such MgO(100) NSs are very flexible. It is necessary to point out that the amplitude of this wavelike NS increases with increasing wavelength and eventually converges to a value of 2.7 Å, when the wavelength of the system reaches 11 times the lattice constant.

The formation energies with different lattice parameters for the MgO(111), MgO(100)-rumpling, and MgO(100)-wave sheets are shown in Figure 2. In Figure 2, one can see clearly

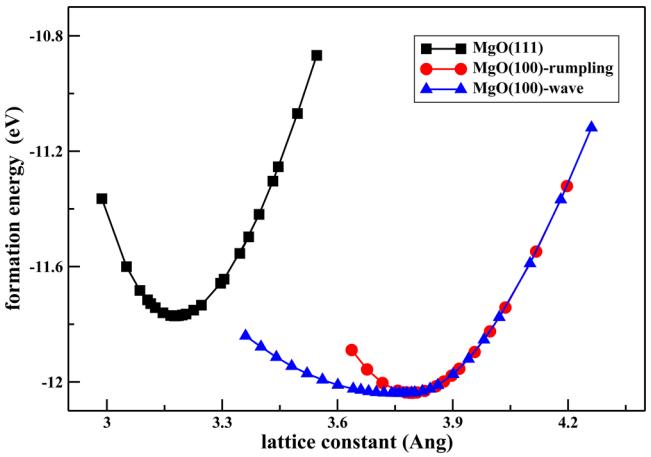

Figure 2. (Color online) Formation energies of the MgO (111) (black), MgO(100)-rumpling (red) and MgO(100)-wave (blue) nanosheets (eV/MgO formula unit), as a function of the lattice constant.

that the MgO(100) NSs with both the rumpling feature and the wavelike feature are much more stable than that of the MgO(111) NS, which implies that the four-coordinate (100) NSs are more stable than the three-coordinate (111) NS. This result is similar to that of germanene (the germanium analogue of graphene)[31] that was predicted recently by using first-principles calculations.

The calculated electronic structures for these MgO NSs show that all of these sheets exhibit semiconductive properties. The band gaps for the MgO(111), MgO(100)-rumpling, and MgO(100)-wave sheets are 4.29, 4.23, and 4.38 eV, respectively. Moreover, we explore the dependence of the band gap on the strain (reflecting in the changes in the lattice parameters). As obviously shown in Figure 3, the band gap of the MgO(111) NS increases linearly as the lattice constant decreases. This is similar to the situation reported in graphitic GaN films.[32] In contrast, for the MgO(100) NS, the band gaps for both the rumpling and the wavelike structures display parabolic trends with the lattice constants. The band gaps reach their maximum values at the equilibrium lattice parameters. The band gap curve for the wave NS coincides with that of the rumpling NS for the stretched lattice parameters, which is attributed to the fact that the wave structure converts to the rumpling one when the lattice constant exceeds 3.84 Å.

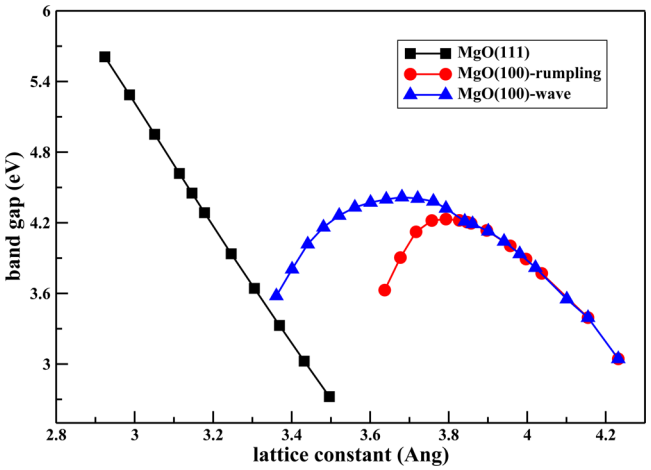

Figure 3. (Color online) The modulation of the band gap of MgO (111) (black), MgO(100)-rumpling (red) and MgO(100)-wave (blue) nanosheets by the strain(lattice constant).

Physically, such a parabolic trend is essentially related to the interaction between Mg and O atoms in these special structures. For either the rumpling sheet or the wave sheet, the distance between Mg and O atoms increases when the NS is stretched, and the interactions between Mg and O atoms become weak. This causes an upward shift of the oxygen energy levels that contribute to the valence band maximum (VBM) and a downward shift of the magnesium energy levels that contribute to the conductive band minimum (CBM). As a result, the band gap becomes narrow. Conversely, the reduction of the lattice constant brings the atoms closer to each other along the direction parallel to the plane, but at the same time, the atoms are farther away from each other along the perpendicular direction of the NS. The net effect is that the distance between Mg and O atoms becomes larger than that of the unconstrained NS, which eventually induces the decrement of the band gap. It is worth noting that, when the lattice constant is stretched over 4.19 Å, both the wave structure and the rumpling structure convert to the planar ones. Therefore, the band gap of the sheet decreases linearly as the lattice constant increases to 4.19 Å, which can be seen in Figure 3.

To check the stabilities of MgO(100) with the rumpling feature and the wavelike feature in multilayers, we optimize these two configurations with double layers and multilayers. The results show that even in double layers both the rumpling sheet and the wave sheet convert to flat ones. This means that the rumpling and wave characteristics exist only in the MgO(100) monolayer.

B. MgO(111) and MgO(100) Nanobelts. We now investigate the stabilities and the electronic properties of the MgO nanobelts (NBs). Like the quasi-1D graphene ribbons with either armchair or zigzag edges, the NB obtained from the hexagonal Mg(111) NS also possesses these two kinds of edges, as shown in Figures 4a and 5a. We denote the MgO(111) NB with armchair edges as MgO(111)-NB-arm and that with zigzag edges as MgO(111)-NB-zig. Following the previous notation for graphene ribbons,[33,34] the notation for the width of the MgO(111)-NB-arm is N_a, and that of MgO(111)-NB-zig is N_z, as marked in Figures 4a and 5a. For the case of MgO(111)-NB-arm, seven different widths of N_a = 2, 3, 4, 6, 9, 12, and 15 are considered, which correspond to widths of 6.39, 9.58, 12.77, 19.04, 28.59, 38.04, 45.97 Å, respectively.

dx.doi.org/10.1021/jp3077062 | J. Phys. Chem. C 2012, 116, 23130−23135

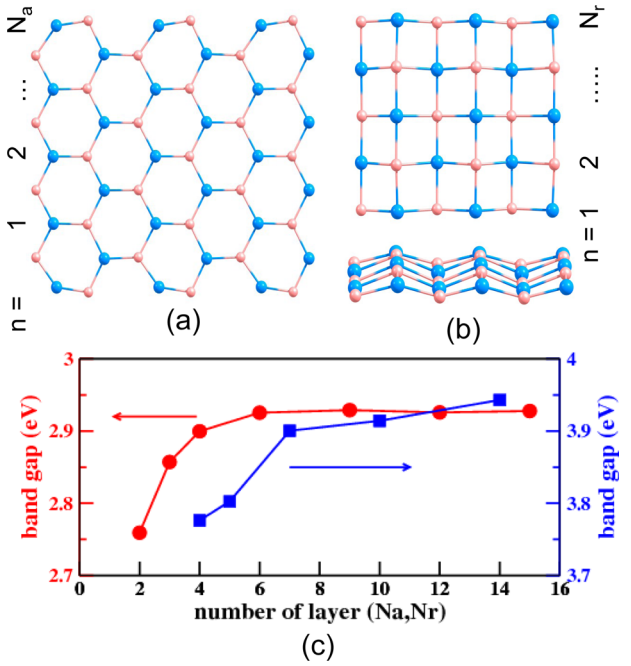

Figure 4. (Color online) The atomic structure of the MgO(111) nanobelt with armchair edges (a), top view (upper) and side view (lower) of the MgO(100)-rumpling nanobelt (b), and the band gaps of the MgO(111)-NB-arm (red) and the MgO(100)-rumpling (blue) nanobelts as the function of the width (c). The blue balls and the red balls in (a) and (b) represent the Mg and the O atoms, respectively.

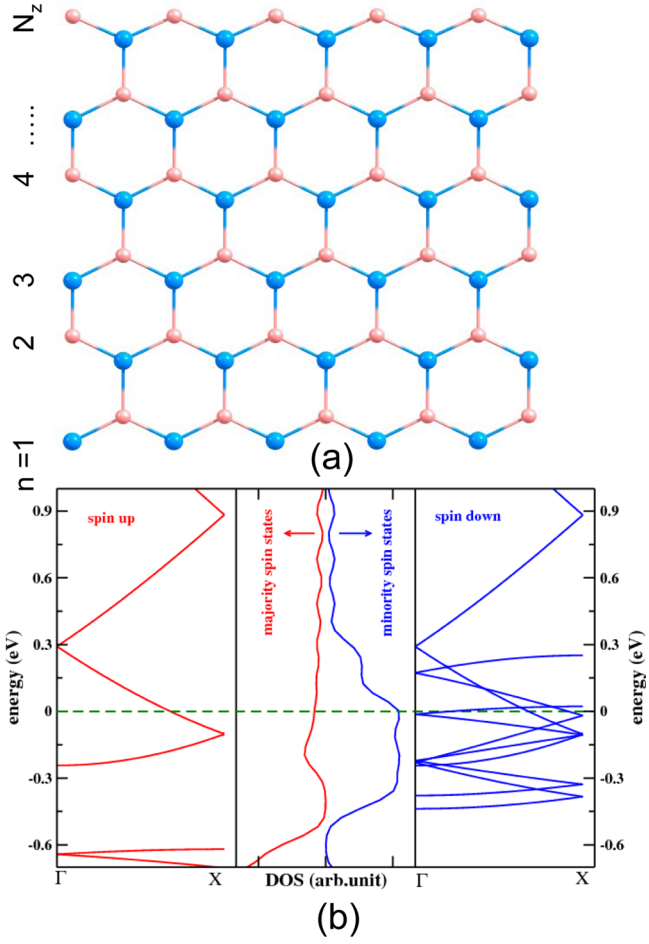

Figure 5. (Color online) The atomic structure of the MgO(111)-NB-zig (a), and the band structures and density of states (DOS) for a typical case with N_z = 6 (b). The blue balls and the red balls in (a) represent the Mg and the O atoms respectively.

The formation energy for MgO(111)-NB-arm decreases from −10.48 to −11.56 eV per Mg−O pair, with N_a varying from 2 to 15. This indicates that as the width increases, the MgO(111)-NB-arm becomes energetically preferable. Our calculations show that all cases of MgO(111)-NB-arm display semiconductive behavior. The band gaps of these NBs are smaller than that of the related NS and strongly depend on their widths, as shown in Figure 4b. For the case of N_a = 2, the band gap is about 2.76 eV. With increasing width of the NB, the band gap increases gradually and reaches 2.93 eV for N_a = 6. The band gap remains at almost this value even for N_a = 15. This implies that the band gap of MgO(111)-NB-arm converges to be about 2.93 eV for N_a > 6. Such a range of band gaps indicates that NBs have promising applications in ultraviolet photoelectronic devices.

For the cases of MgO(111)-NB-zig, six different widths with N_z = 2, 4, 6, 9, 12, and 16 (corresponding to 2.0, 9.06, 14.35, 22.68, 30.94, and 41.98 Å in width) are taken into account. Compared to MgO(111)-NB-arm, MgO(111)-NB-zig shows different structural features. For each case of MgO(111)-NB-arm (Figure 4a), both edges consist of Mg−O dimers being equivalent to each other. In contrast, for each case of MgO(111)-NB-zig, the edges are composed of Mg and O atoms, as shown in Figure 5a. After optimization, we find that the hexagonal MgO(111)-NB-zig with N_z = 2 converts to a flat, square MgO(100) structural feature, with separated Mg and O in the hexagon bonding to each other. For Mg(111)-NB-zig with N_z > 2, the hexagonal symmetry remains after full relaxation. For each stable case of Mg(111)-NB-zig, the formation energy decreases from −10.60 to −11.47 eV as N_z increases from 4 to 16. This implies that Mg(111)-NB-zig with larger N_z is more energetically favorable.

Different structural features result in different electronic properties. Our calculations show that the case of N_z = 2 exhibits semiconducting behavior with a band gap of 4.10 eV, and the other cases display metallic properties. Moreover, we find that the spin splitting appears in the calculated density of states (DOS), and both the majority and minority spin states run across the Fermi level. A typical case with N_z = 6 is shown in Figure 5b. Further analysis reveal that the majority spin states below the Fermi level mainly come from the contribution of 2p orbitals of the O atoms at the edges whereas the minority spin states come from the hybridization of Mg 2s and O 2p orbitals of the outmost atoms at the opposite edges.

The splitting of the majority spin states and the minority spin states brings the magnetic moment into the system. Moreover, we find that the magnetic moment of the system increases, with increasing width of the NB. For example, the magnetic moments of the systems with N_z = 4, 6, 9, 12, and 16 are 2.20μ_B, 2.62μ_B, 3.13μ_B, 3.25μ_B, and 3.35μ_B, respectively. Further investigations indicate that such an increment results from two factors: on the one hand, with increasing width of the NB, the distance between the Mg and O atoms at the opposite edges increases. Consequently, the hybridization of Mg 2s and O 2p orbitals becomes weak, and the minority spin states that mainly come from the hybridization of Mg 2s and O 2p orbitals decrease accordingly. On the other hand, as the width increases,

dx.doi.org/10.1021/jp3077062 | J. Phys. Chem. C 2012, 116, 23130−23135

besides the O atoms at the outmost edge, the O atoms near the edge are also polarized, also making a contribution to the majority spin states. This enhances the majority spin states directly. As a result, a combination of the enhancement of the majority spin states and the decrement of the minority spin states leads to the increment of the magnetic moment.

For the rumpling and wavelike MgO(100) NBs, the widths of the NBs are denoted as N_r, as shown in Figure 4c. For these two kinds of NBs, six different widths, N_r = 2, 4, 5, 7, 10, and 14, are considered, which respectively correspond to widths of 1.81, 5.80, 7.64, 11.46, 17.28, and 24.95 Å of the NBs. After full optimization, the rumpling NBs with N_r = 2 become a flat one, just like the MgO(111)-NB-zig with N_z = 2. For the NBs with N_r = 4, 5, 7, 10, and 14, the buckling features get more striking along the periodic direction, as compared to that of the MgO(100)-rumpling NSs, and the distance between the buckling atoms along the z direction reaches about 0.41 Å. In contrast, such a buckling feature disappears along the nonperiodic direction. As a representative, the side view of the NB with N_r = 5 is shown in Figure 4c. For the wavelike NBs, we unexpectedly find that they are optimized to the same cases of the rumpling ones. Similar to the cases of Mg(111)-NB-arm and Mg(111)-NB-zig, such optimized MgO(100) rumpling NBs become more stable as the width increases. The corresponding formation energy decreased from −10.58 to −11.84 eV when N_r increased from 4 to 14

Similar to the cases of MgO(111)-NB-arm, the optimized MgO(100)-rumpling NBs exhibit semiconductive properties. Likewise, with increasing width of the nanobelt, the band gap increases accordingly, as shown in Figure 4b. For N_r = 4, the band gap of the NBs is about 3.75 eV, and it increases rapidly to 3.90 eV for N_r = 7. Then, it increases slowly from N_r = 7 to 14 and reaches 3.95 eV for N_r = 14. This is obviously shown in Figure 4b.

From the calculations above, we predict that the MgO nanobelts, with either metallic properties or tunable band gaps by the width of the belts, possess great potential applications in spintronics and nanoscaled photoelectronic devices.

IV. SUMMARY

By using first principles calculations, we predict the stabilities and electronic properties of MgO NSs and the corresponding NBs. We find that the nonpolar MgO(100) NSs energetically prefer to be with either the rumpling or the wavelike features, rather than the flat one. Both the MgO(111) NS and the MgO(100) NSs exhibit semiconductive properties, with band gaps of between 4.23 and 4.38 eV. Moreover, MgO(111) NBs with zigzag edges show metallic behavior, whereas that with armchair edges shows semiconductive properties. Meanwhile, the MgO(100) NBs also exhibit semiconductive properties. The band gaps for both Mg(111)-NB-arm and MgO(100) NBs can be significantly tuned by their widths. The metallic behaviors and the tunable band gaps provide these MgO NBs with promising applications in spintronics and ultraviolet optielectronic devices.

AUTHOR INFORMATION

Corresponding Author

*E-mail: hyhe@ustc.edu.cn.

Notes

The authors declare no competing financial interest.

ACKNOWLEDGMENTS

This work is supported by the National Science Foundation of China (grant no. NSFC11105140), the Anhui Provincial Natural Science Foundation (no. 11040606M17), and the National Basic Research Program of China (grant no. 2009CB939901). The HP-LHPC of USTC is acknowledged for computational support. B.C.P. is grateful for the support of the Ph.D. programs foundation of the Ministry of Education of China.

REFERENCES

(1) Bolotin, K. I.; Ghahari, F.; Shulman, M. D.; Stomer, H. L.; Kim, P. *Nature* **2009**, *62*, 196−199.
(2) Zhang, Y.; Tan, Y.-W.; Stormer, H. L.; Kim, P. *Nature* **2005**, *438*, 201−204.
(3) Lin, Y.; Böker, A.; He, J.; Sill, K.; Xiang, H.; Abetz, C.; Li, X.; Wang, J.; Emrick, T.; Long, S.; Wang, Q.; Balazs, A.; Russell, T. P. *Nature* **2005**, *434*, 55−59.
(4) Fang, X.; Bando, Y.; Gautam, U. K.; Ye, C.; Golberg, D. *J. Mater. Chem.* **2008**, *18*, 509−522.
(5) Goniakowski, J.; Noguera, C.; Giordano, L. *Phys. Rev. Lett.* **2004**, *93*, 215702−215705.
(6) Yan, H.; Choe, H. S.; Nam, S. W.; Hu, Y.; Das, S.; Klemic, J. F.; Ellenbogen, J. C.; Lieber, C. M. *Nature* **2011**, *470*, 240−244.
(7) Obradovic, B.; Kotlyar, R.; Heinz, F.; Matagne, P.; Rakshit, T.; Giles, M. D.; Stettler, M. A.; Nikonov, D. E. *Appl. Phys. Lett.* **2006**, *88*, 142102−142104.
(8) Katsneson, M. I.; Novoselov, K. S.; Geim, A. K. *Nat. Phys.* **2006**, *2*, 620−625.
(9) Takeda, K.; Shiraishi, K. *Phys. Rev. B* **1994**, *50*, 14916−14922.
(10) Yang, P. D.; Lieber, C. M. *Science* **1996**, *273*, 1836−1840.
(11) Choudary, B. M.; Ranganath, K. V. S.; Pal, U.; Kantam, M. L.; Sreedhar, B. *J. Am. Chem. Soc.* **2005**, *127*, 13167−13171.
(12) Selvamani, T.; Sinhamahapatra, A.; Bhattacharjya, D.; Mukhopadhyay, I. *Mater. Chem. Phys.* **2011**, *129*, 853−861.
(13) Hayashi, K.; Matsuishi, S.; Kamiya, T.; Hirano, M.; Hosono, H. *Nature* **2002**, *419*, 462−465.
(14) Kim, J.; Gila, B.; Mehandru, R.; Johnson, J. W.; Shin, J. H.; Lee, K. P.; Luo, B.; Onstine, A.; Abernathy, C. R.; Pearton, S. J.; Ren, F. J. *J. Electrochem. Soc.* **2002**, *149*, G482−G484.
(15) Novoselov, K. S.; Geim, A. K.; Morozov, S. V.; Jiang, D.; Katsnelson, M. I.; Grigorieva, I. V.; Dubonos, S. V.; Firsov, A. A. *Nature* **2005**, *438*, 197−200.
(16) Itzykson, C.; Zuber, J.-B. *Quantum Field Theory*; Dove: New York, 2006.
(17) Calogeracos, A.; Dombey, N. *Contemp. Phys.* **1999**, *40*, 313−321.
(18) Berger, C.; Song, Z. M.; Li, X. B.; Wu, X. S.; Brown, N.; Naud, C.; Mayou, D.; Li, T. B.; Hass, J.; Marchenkov, A. N.; Conrad, E. H.; First, P. N.; de Heer, W. A. *Science* **2006**, *312*, 1191−1196.
(19) Matsuzaki, K.; Hosono, H.; Susaki, T. *Phys. Rev. B* **2010**, *82*, 033408−033411.
(20) Chen, T. L.; Li, X. M.; Yu, W. D.; Zhang, X. *Appl. Phys. A: Mater. Sci. Process.* **2005**, *81*, 657−661.
(21) Goniakowski, J.; Noguera, C. *Phys. Rev. B* **2009**, *79*, 155433−155437.
(22) Pan, Y.; Benedetti, S.; Nilius, N.; Freund, H.-J. *Phys. Rev. B* **2011**, *84*, 075456−075460.
(23) Ordejón, P.; Artacho, E.; Soler, J. M. *Phys. Rev. B* **1996**, *53*, R10441−R10444.
(24) Sánchez-Portal, D.; Ordejón, P.; Artacho, E.; Soler, J. M. *Int. J. Quantum Chem.* **1997**, *65*, 453−461.
(25) Soler, J. M.; Artacho, E.; Gale, J. D.; García, A.; Junquera, J.; Ordejón, P.; Sánchez-Portal, D. *J. Phys.: Condens. Matter* **2002**, *14*, 2745−2779.
(26) Troullier, N.; Martins, J. L. *Phys. Rev. B* **1991**, *43*, 1993−2006.

(27) Kleinman, L.; Bylander, D. M. *Phys. Rev. Lett.* **1982**, *48*, 1425−1428.
(28) Bylander, D. M.; Kleinman, L. *Phys. Rev. B* **1990**, *41*, 907−912.
(29) Giordano, L.; Goniakowski, J.; Pacchioni, G. *Phys. Rev. B* **2003**, *67*, 045410−045417.
(30) Mao, Y. D.; Wang, W. L.; Wei, D.; Kaxiras, E.; Sodroski, J. G. *ACS Nano* **2011**, *5*, 1395−1400.
(31) Cahangirov, S.; Topsakal, M.; Aktürk, E.; Sahin, H.; Ciraci, S. *Phys. Rev. Lett.* **2009**, *102*, 236804−236807.
(32) Wu, D. X.; Lagally, M. G.; Liu, F. *Phys. Rev. Lett.* **2011**, *107*, 236101−236105.
(33) Abanin, D. A.; Lee, P. A.; Levitov, L. S. *Phys. Rev. Lett.* **2006**, *96*, 176803−176806.
(34) Son, Y.-W.; Cohen, M. L.; Louie, S. G. *Phys. Rev. Lett.* **2006**, *97*, 216803−216806.